An Aerosol Climatology at Kyoto: Observed Local Radiative Forcing and Columnar Optical Properties

TAKAHIRO YABE,* ROBERT HÖLLER,+ SUSUMU TOHNO, AND MIKIO KASAHARA

Graduate School of Energy Science, Kyoto University, Kyoto, Japan

(Manuscript received 26 March 2002, in final form 23 October 2002)

ABSTRACT

In order to evaluate the radiative effect of the atmospheric aerosol at Kyoto, Japan, surface solar irradiance and columnar aerosol optical properties were observed in the period between September 1998 and December 2001. The aerosol optical thickness, which is an indicator of the columnar mass burden and the overall radiative effect of the aerosol, was on average 0.27 at a wavelength of 500 nm. Springtime aerosol optical thickness was generally higher primarily because of ''yellow dust'' from the Asian continent. The Ångström exponent had values ranging from 0.5 to 2.8, with an average value of 1.64, and was found to be low in periods during which the aerosol optical thickness was high. As a first step toward calculating the local climate impact of the atmospheric aerosol at Kyoto, the clear-sky direct radiative forcing is considered in this paper. For an evaluation of the surface aerosol radiative forcing, observed total surface fluxes measured by a pyranometer are subtracted from modeled surface fluxes derived from a non-aerosol-laden atmosphere. From the obtained relationship between the aerosol optical thickness and the surface aerosol radiative forcing, it is concluded that there is a high variability in the physical and chemical characteristics of the aerosol at this location. The surface radiative forcing efficiency, which is the radiative forcing for unit optical thickness, was -85.4 W m^{-2} on average at Kyoto. This observed value is very similar to recently observed surface aerosol radiative forcings during the Indian Ocean Experiment (INDOEX) and the Asia Pacific Regional Aerosol Characterization Experiment (ACE-Asia) field campaigns. The aerosol radiative forcing at the top of the atmosphere (TOA) was calculated from measured in situ aerosol optical properties and retrieved properties from a comparison of measured and simulated ground solar irradiances. While employing average aerosol optical properties at Kyoto, comprehensive cooling at the TOA was found. It was also found that the difference between the surface and the TOA aerosol radiative forcings produced a large amount of atmospheric heating because of the relatively low single-scattering albedo. Surface forcing was about 3 times as high as the TOA forcing at Kyoto. The main conclusion of this study is that the aerosol over Kyoto significantly alters the atmospheric energy budget. The aerosol is highly variable in terms of its optical properties, so that a highly nonlinear relationship exists between the surface radiative forcing and the aerosol optical thickness.

1. Introduction

It has been widely recognized that natural and anthropogenic aerosols play an important role in the earth's climate system (Chylek and Coakley 1974). Aerosol radiative forcing, which can be divided into a direct part that is caused by scattering and absorption of solar and longwave radiation by particles, and an indirect part that originates from the interaction of aerosols with clouds, is comparable, but opposite in sign, to the radiative forcing of the greenhouse gases (Houghton et al. 2001). An evaluation of the aerosol radiative forcing on a global scale is, however, highly uncertain because of uncertainties in the optical properties and the spatial distribution of the aerosol (Charlson et al. 1992; Schwartz 1996; Hansen et al. 1997). Recently, large field campaigns such as the Tropospheric Aerosol Radiative Forcing Observational Experiment (TARFOX) (Russell et al. 1999), the Indian Ocean Experiment (INDOEX) (Ramanathan et al. 2001), and the Asia Pacific Regional Aerosol Characterization Experiment (ACE-Asia) (Huebert et al. 2003, manuscript submitted to *J. Geophys. Res.*) attempted the first integrated field studies with the aim of measuring both the physical and chemical properties and the resulting radiative forcing of the atmospheric aerosol. Still, more case studies of aerosol optical properties and associated radiative effects are necessary to constrain the impact of anthropogenic aerosols on the climate system, both on local and global scales.

So far, most studies of the aerosol radiative effect have concentrated on sulfate aerosols (Charlson et al.

* Current affiliation: New Energy and Industrial Technology Development Organization (NEDO), Tokyo, Japan.

+ Current affiliation: Earth Observation Research Center, National Space Development Agency of Japan, Tokyo, Japan.

Corresponding author address: Robert Höller, Earth Observation Research Center, National Space Development Agency of Japan, Triton Square X 22F, 1-8-10 Harumi, Chuo-ku, Tokyo, Japan.
E-mail: hoeller@eorc.nasda.go.jp

© 2003 American Meteorological Society

Unauthenticated | Downloaded 05/06/21 04:29 AM UTC

1992), because they make a large contribution to the anthropogenic aerosol and efficiently scatter solar radiation. Only recently has attention been paid to other types of particles, such as carbonaceous aerosols (Haywood and Shine 1995; Russell et al. 1999; Sateesh et al. 1999; Takemura et al. 2002). In particular, absorbing materials such as black carbon play an important role in radiative forcing estimates, because the single-scattering albedo is highly sensitive to trace absorbing species in the atmosphere (Horvath 1993; Pilinis et al. 1995). Carbonaceous aerosols have also been reported to be a major component of the atmospheric aerosols in Japan (Ohta and Okita 1984; Höller et al. 2002). Moreover, the radiative influence of carbonaceous aerosols is very complex, because they can produce a cooling at the surface, warming in the atmosphere, and both cooling or heating at the top of the atmosphere (TOA), depending on the single-scattering albedo of the particles. In an earlier work we performed continuous measurements of particulate matter with a mass median aerodynamic diameter of less than 10 μm (PM-10) and carbonaceous aerosols at Kyoto, Japan. Höller et al. (2002) found that carbonaceous aerosols account for 37% of the total aerosol mass concentration and that the ratio of elemental carbon to total carbon aerosol is about 0.6. This means that a high fraction of the aerosol at this location is absorbing and can, therefore, have a significant influence on the radiative balance of the surface–atmosphere system.

Simultaneous measurements of solar radiation and aerosol optical properties have already been performed in order to estimate the radiative effect of the atmospheric aerosol (Conant et al. 1997; Russell et al. 1999; Hignett et al. 1999; Satheesh et al. 1999; Podgorny et al. 2000). In all of these cases, the anthropogenic aerosols were cooling the atmosphere at the surface and the TOA, while heating the atmosphere to a considerable extent through absorption of solar radiation. Only purely scattering aerosols lead to cooling at the TOA without heating the atmosphere.

Here we emphasize the necessity to understand aerosol optical properties and aerosol-related radiative effects in Japan. This is because in such a highly industrialized country with a complex variety of anthropogenic and natural aerosol sources, the aerosol optical properties are expected to have a large variability. Moreover, the meteorological patterns in Japan are seasonally influenced by long-range transport of dust particles and pollution from the Asian continent, which usually takes place in the lower free troposphere (Iwasaka et al. 1983; Hirose et al. 1983). Given the predicted increase in emissions in China, it clearly becomes important to study the aerosol optical properties and associated radiative impacts on a long-term basis at several locations in the Asian–Pacific region. With this in mind, the objectives of this study are as follows: 1) describing continuous measurements of surface irradiance and columnar aerosol optical properties (information on the chemical composition and in situ optical properties of the aerosols is taken from long-term measurements or intensive campaigns at the same location) (Höller 2000; Höller et al. 2000); 2) comparison of the radiative transfer calculations with surface irradiance measurements; 3) estimation of the aerosol radiative forcing at the surface, the top of the atmosphere, and in the atmosphere; 4) discussion of the columnar aerosol optical properties and the range of surface radiative forcing on the basis of the derived relationship between the aerosol optical thickness and the surface radiative forcing, together with comparison with radiative transfer calculations using model aerosols, and 5) comparison of the results of this study with observations of aerosol radiative forcing at other locations.

2. Instrumentation and measurements

Measurements of surface solar irradiance and columnar aerosol optical properties were performed at the Uji campus (34°54′N, 135°48′E) of Kyoto University, which is located in a suburban/residential area in the southeast of Kyoto, Japan. A highway passes to within about 1 km south of the campus, but no major aerosol sources are located nearby. The period of data analyzed for this work is from September 1998 to December 2001. A multiwavelength sun photometer (EKO MS-110A) mounted on a sun tracker was used to retrieve the aerosol optical thickness by measuring the attenuation of direct solar radiation at wavelengths $\lambda = 368$, 500, 675, and 778 nm. Aerosol optical thickness $\tau_{a\lambda}$ is calculated from

$$\tau_{a\lambda} = \frac{1}{m} \ln \frac{I_{0\lambda}}{I_{\lambda}} - \tau_{0\lambda} - \tau_{R\lambda}, \tag{1}$$

where $I_{0\lambda}$ is the direct solar irradiance at the top of the atmosphere, I_{λ} is the measured direct solar irradiance, $\tau_{0\lambda}$ is the ozone optical thickness, $\tau_{R\lambda}$ is the optical thickness of the air molecules, and m is the solar optical air mass. To obtain $I_{0\lambda}$, the instrument must be calibrated. This operation was carried out by a comparison of the instrument with a standard sun photometer owned by the Japanese Meteorological Research Institute, located in Tsukuba. The instrument was calibrated once per year and was regularly cleaned. The solar optical air mass m at the solar zenith angle θ is calculated from (Kondratyev 1969)

$$m = \frac{1}{\sin\theta + 0.15(\theta + 3.885)^{-1.253}}. \tag{2}$$

The Rayleigh optical thickness of the air molecules was obtained from Young (1981). For a calculation of τ_0, a columnar ozone amount of 0.3 cm as an average value for this site is assumed, which is supported by measurements by the Japan Meteorological Agency at Tsukuba, using Dobson spectrometers (Japan Meteorological Agency 2002). Because the ozone concentration has

Unauthenticated | Downloaded 05/06/21 04:29 AM UTC

only weak influence on the aerosol optical thickness retrieval, the daily and seasonal variation of the ozone amount was not taken into account. Absorption of other gases than ozone was neglected in the analysis, because the effect on the analysis of aerosol optical thickness is small.

For measurements of the direct and total downward solar flux F (W m^{-2}), a pyrheliometer (EKO MS-53) and a pyranometer (EKO MS-801) were used, respectively. The pyrheliometer measures the downwelling direct solar flux between 0.3 and 2.8 μm, and the pyranometer measures the downwelling total flux between 0.305 and 2.8 μm. The diffuse solar irradiance is obtained by subtracting the direct irradiance from the total irradiance. Although the wavelength range of the two instruments is slightly different, it was not taken into account here because of its negligible influence on the flux measurement. Measurements of global fluxes might be overestimated, especially for high solar zenith angles, because of the directional response of the pyranometer (Satheesh et al. 1999). The pyranometer has an accuracy of 5%, but the error can reach ± 10 W m^{-2} because of the directional response of the instrument. The sensing element consists of a wire-wound thermopile, covered with black paint that has a spectrally flat absorption response. The manufacturer guarantees that temperature and nonlinearity account for less than 1% of the total error up to 50°C. There might be additional systematic errors due to radiative transfer between the domes and the detector of the pyranometer, but these effects were not taken into account here (Bush et al. 2000). The effects of flux measurement errors on the derived aerosol radiative forcing estimates are discussed in section 5.

Automatic observation of direct solar fluxes with a sun-tracking system faces the problem that clouds move through the line of sight and produce false optical thickness data. Therefore, automated observation requires a cloud-screening procedure. Because we continuously observe both direct and global irradiances, we are able to identify periods of hemispherically clear (i.e., cloudless) skies from the known characteristics of a typical clear-sky irradiance time series. The Ångström exponent is used as an additional check to avoid measuring the optical thickness of a thin cloud layer. In such a case, the optical thickness does not differ significantly from an aerosol layer, but the Ångström exponent has much lower values, which reveal larger cloud droplets.

3. Radiative transfer calculations

Direct aerosol radiative forcing at the surface is defined as the difference between the observed net flux and the calculated ''no-aerosol'' net flux. Necessary fluxes for a non-aerosol-laden atmosphere were calculated using the moderate-resolution atmospheric radiance and transmittance model and code (MODTRAN4), which employs a correlated-k algorithm and the discrete ordinate radiative transfer (DISORT) multiple-scattering model for improved multiple-scattering calculations (Berk et al. 1999). Fluxes were calculated with a spectral grid of 1 cm^{-1}. The model includes molecular Rayleigh scattering, gaseous absorption, aerosol, and cloud effects. Because we focus on the direct aerosol radiative forcing under clear skies, clouds are not considered in this study. The *U.S. Standard Atmosphere, 1976* was used for the vertical profiles of pressure and gases other than carbon dioxide (CO_2), water vapor, and ozone. The CO_2 mixing ratio was set at 380 ppmv, employing data from the Japan Meteorological Agency. Simulated clear-sky fluxes are sensitive to solar zenith angle, surface albedo, and atmospheric profiles of humidity, aerosols, and ozone. A columnar ozone concentration of 0.3 cm was used, which is an annual average value observed at Tsukuba, the nearest observation site of the Japan Meteorological Agency to Kyoto. The ozone concentration there has a seasonal cycle ranging between 0.25 and 0.35 cm (Japan Meteorological Agency 2002). However, the influence of the ozone concentration on the total surface flux was found to be small. A sensitivity analysis showed that a 20% change in the ozone concentration results in a less than 0.5% change in the simulated surface irradiance.

For the surface albedo, we employed a value of 0.15 for calculations of the upward flux. With the exception of a few days per year, Kyoto has no snow cover, so the surface albedo could be treated as a constant. However, we also performed albedo measurements of several surfaces, using an albedometer (EKO MR-22) with a spectral range of 300–2800 nm, and found surface albedo values ranging between 0.13 and 0.17, depending on the surface type and the zenith angle. We therefore regard 0.15 ± 0.2 as appropriate for Kyoto with respect to the latitude and vegetation cover. This value is also consistent with reported surface albedo values of cities with similar latitudes in the United States (Iqbal 1983). A discussion of the influence of the error of the surface albedo on the obtained radiative forcing is given in section 5.

The total precipitable water vapor, which is necessary to calculate clear-sky fluxes, was obtained from Global Positioning System (GPS) measurements, using data from the Geographical Survey Institute in Japan. Because GPS data were not available for the whole period of observation of solar irradiance, the number of available days for an evaluation of the clear-sky radiative forcing was limited. The error of the retrieved water vapor from the GPS data is within ± 2 mm (Tregoning et al. 1998), and we use this value in an error analysis of the calculated clear-sky fluxes in section 5.

MODTRAN4 is not only used to calculate solar irradiance for a non-aerosol-laden atmosphere, but also to compare measured with simulated solar irradiance at the surface. In that case the problem is more complicated, because values for the aerosol optical and physical parameters are needed as input parameters. In MODTRAN4, several kinds of boundary layer aerosol

Unauthenticated | Downloaded 05/06/21 04:29 AM UTC

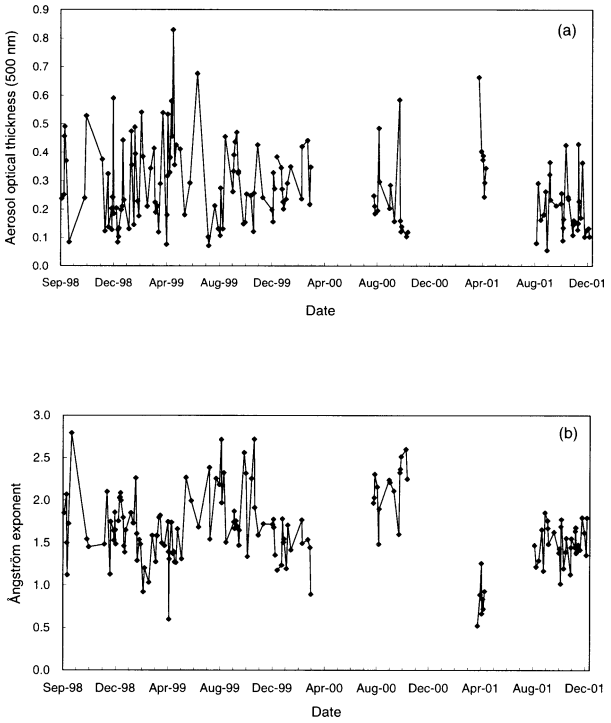

FIG. 1. Time series of (a) daytime-averaged aerosol optical thickness at 500 nm and (b) Ångström exponents in the period between Sep 1998 and Dec 2001 at Kyoto, Japan.

models with defined optical properties can be chosen. The urban and rural aerosol models were used as a reference to compare the calculated aerosol radiative forcing with the observation. The default urban model has a single-scattering albedo ω_0 of 0.64 and an asymmetry parameter g of 0.66 at 500 nm, while the default rural model ω_0 is 0.94 and g is 0.65 at the same wavelength. The optical parameters of the default models can be changed for all wavelengths using a scaling factor at 500 nm or by employing detailed wavelength-dependent aerosol optical properties. In section 4 the columnar aerosol single-scattering albedo is retrieved from a comparison of measured and simulated values of solar irradiance at the ground. Especially the diffuse irradiance is very sensitive to aerosol absorption, which makes a retrieval of the single-scattering albedo possible. This value is then used to estimate the TOA radiative forcing.

4. Results

a. Solar irradiance and aerosol optical properties

Time series of daytime averages of the aerosol optical thickness $\tau_{a,500}$ at 500 nm and the Ångström exponent α observed at Kyoto in the period between September 1998 and December 2001 are shown in Fig. 1. Between 23 March and 7 August 2000 and between 27 April and 16 August 2001 no data are available, because of calibration and maintenance of the instruments and a technical problem with the sun-tracking system. Between 19 March and 6 April 2001 the instrumentation was used at a coastal site on the Sea of Japan during the ACE-Asia intensive field campaign; therefore, no data are available at the Kyoto site during this period. Ångström exponents α are calculated from optical thickness values τ_a at wavelengths 368 and 675 nm by

$$\alpha = -\frac{\log(\tau_{a,368}/\tau_{a,675})}{\log(368/675)}. \quad (3)$$

Higher Ångström exponents indicate smaller aerosol particles, and vice versa. We analyzed a total of 155 daytime averages and found average $\tau_{a,500}$ values to have a high fluctuation between 0.06 (September 2001) and 0.83 (May 1999), whereas monthly average values were between 0.20 (January 1999) and 0.64 (July 1999). The average of $\tau_{a,500}$ during the whole measurement period is 0.27, which is quite typical for a suburban site and is comparable to suburban sites of the aerosol robotic network (AERONET) (Holben et al. 2001).

Ångström exponent values generally range from greater than 2.0 for particles near combustion sources to values smaller than zero for coarse-mode-dominated desert dust aerosols. At Kyoto we found daily average α values ranging from 0.52 (April 2001) to 2.79 (September 1998), with an annual mean value of 1.64. Both the springtime of 2000 and of 2001 showed high optical thickness values, and at the same time lower values of the Ångström exponent. This indicates higher concentrations of coarse aerosols during spring, which is consistent with the common observation of Asian dust (''Kosa'') during springtime in Japan. Atmospheric turbidity is generally low during the winter months and high in the summer. This follows a classical annual pattern, which was also observed by Flowers et al. (1969) and Holben et al. (2001). Increases of optical thickness can be explained by an increased concentration of aerosol sources processed by convection by humid air masses.

A scatterplot of $\tau_{a,500}$ versus α is shown in Fig. 2. This plot can be used to characterize the amount and size range of the aerosol and is often used as a ''fingerprint'' of the aerosol at a given location (Nakajima et al. 1996; Holben et al. 2000). Comparing our observations of optical thickness and Ångström exponents with data from AERONET sites (Holben et al. 2001), we find that Kyoto has the typical characteristics of an urban site with a broad range of α values due to a large variety of aerosol sources. The air above Kyoto is influenced by air masses from the heavy industrialized Osaka Bay area, Pacific air masses during the summertime, and the continental Asian outflow during spring. This results in a large variety of aerosols, which can also have a broad range of optical properties and chemical compositions. It is interesting to note that there are no data points with very small Ångström exponents and, at the same time, small optical thickness values.

Unauthenticated | Downloaded 05/06/21 04:29 AM UTC

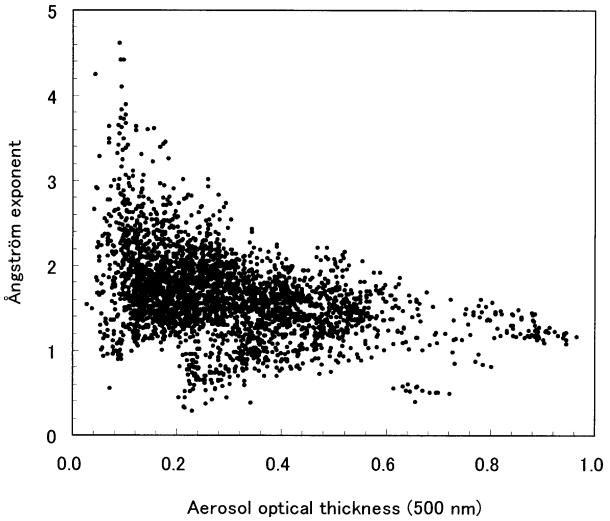

FIG. 2. Scatterplot of the aerosol optical thickness (500 nm) vs Ångström exponents at Kyoto.

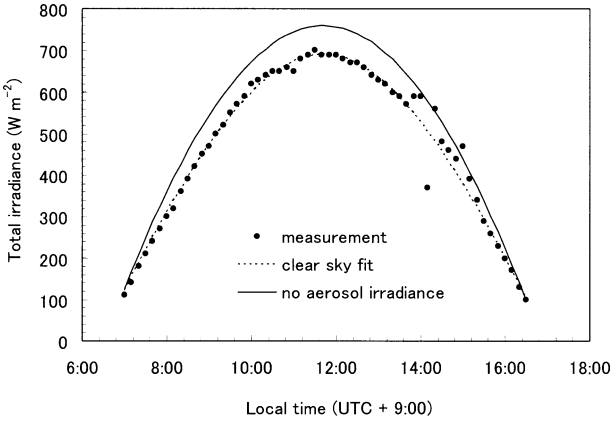

FIG. 3. Time series of measured total surface solar irradiance (W m^{-2}) and simulated no-aerosol total irradiance (19 Oct 2001).

This might be due to the fact that the periods influenced by Asian dust are at the same time influenced by fine particles in the accumulation mode, which could be local pollution or transport of accumulation mode particles from the Asian continent.

Figure 3 shows the measured and simulated total surface solar irradiance for 21 October 2001, which represents typical clear days in Kyoto. The straight line indicates the modeled no-aerosol irradiance calculated by MODTRAN4, using measured precipitable water from GPS. Circles indicate the measured total irradiance noted by the pyranometer, and the dotted line is the clear-sky fit to the measured irradiance. The effect of clouds can be seen in the latter half of the dataset. Clouds can both reduce and enhance the measured irradiance as compared with a clear-sky aerosol-laden atmosphere, because they can block the observed direct flux when directly in the line of sight, but may also increase the irradiance because of scattering from cloud edges (Hayasaka et al. 1995). Cloud layers cover the sky over Kyoto during extended periods throughout the year, which limits observational estimation of the clear-sky radiative forcing to days with only partly cloudy skies. The number of days used for the analysis here was further reduced by the limited availability of GPS data. Therefore, for the estimation of a radiative forcing, only 21 days of the whole dataset were used. These data are not being influenced by thin, uniform cloud layers. A polynomial could therefore be fitted to measured irradiance time series data to obtain the clear-sky irradiance.

b. Calculation of aerosol radiative forcing

Radiative forcing at the TOA is an important indicator when considering the comprehensive energy budget of the atmosphere–surface system. It indicates whether more or less energy is emitted from the globe. Nevertheless, the surface radiative forcing is also an important indicator, because a change in the surface solar flux can change the surface temperature and the evaporation of water vapor, and can therefore have significant influence on the climate system. Here we obtain a surface aerosol radiative forcing from directly observed surface fluxes and calculated no-aerosol irradiances. TOA forcing is estimated from a simulation of TOA fluxes using aerosol optical properties obtained from validated ground fluxes at the surface and in situ measurements.

Surface aerosol radiative forcing ΔF_s is defined as

$$\Delta F_s = F_s^a - F_s^o, \tag{4}$$

where F_s^a and F_s^o are the net fluxes at the surface for aerosol-laden and aerosol-free cases, respectively. TOA radiative forcing ΔF_{TOA} is calculated by

$$\Delta F_{\mathrm{TOA}} = -(F_{\mathrm{TOA}}^a\uparrow - F_{\mathrm{TOA}}^o\uparrow), \tag{5}$$

where $F_{\mathrm{TOA}}^a\uparrow$ and $F_{\mathrm{TOA}}^o\uparrow$ are the upward fluxes at the TOA for the aerosol-laden and aerosol-free cases, respectively (Liao and Seinfeld 1998). Although radiative forcing is defined as the difference of the net fluxes, in Eq. (5) only the upward fluxes are written. The downward flux terms cancel out, because they are the same at the TOA for the aerosol-laden and aerosol-free cases.

TOA fluxes were not directly measured but were rather obtained from radiative transfer calculations. Necessary aerosol parameters for the calculation of aerosol-laden TOA fluxes were obtained from in situ measurements in the case of the asymmetry parameter and the aerosol optical depth. For the size distribution of particles, the urban model's parameterization of MODTRAN4 was employed. Measurements of aerosol size distributions at Kyoto using cascade impactors (Kasahara et al. 1999) showed that the structure of the size distribution of the atmospheric aerosol at Kyoto does not change very much with time and that the urban model size distribution represents the aerosol at our site very well. Still, the use of a fixed aerosol size distri-

Unauthenticated | Downloaded 05/06/21 04:29 AM UTC

bution might induce an error in the simulated fluxes. We regard this error as small because the 8 days we used for the comparison had very stable values in the optical depth and Ångström parameter.

Measured and calculated surface irradiances were compared for 8 cloud-free days. These days also showed very stable atmospheric conditions and low variations of the aerosol optical depth and Ångström exponent values. As an input parameter for the flux simulations, aerosol optical thickness measured by the sunphotometer was used. Aerosol backscattering ratios measured by an integrating nephelometer equipped with a backscatter shutter (TSI, Inc., model 3563) were used to obtain the asymmetry parameter g. Measurements showed that the backscatter ratio b in Kyoto has a range between 0.12 and 0.14 (Höller 2000). The backscattering ratio is the fraction of the scattered intensity that is redirected into the backward hemisphere of the scattering particle. There is generally no one-to-one relationship between the asymmetry parameter g and b, because the relationship depends on the size distribution and refractive index of the particles (Marshall et al. 1995). For the radiative transfer calculations an asymmetry parameter of 0.65 was employed, which was obtained from Mie simulations for an aerosol with an urban model size distribution; $b = 0.13$ was obtained as an average value from nephelometer measurements during the 8 days of observation. In situ measurements at Kyoto showed that the single-scattering albedo ω_0, which has a significant influence on the diffuse sky irradiance, shows a strong variability there. Value of ω_0 varied between 0.6 and 0.98, with an average value of 0.85 for 30 days of measurement (Höller et al. 2000). This is also confirmed by the strong variation of the elemental carbon (EC) concentration at this site (Höller et al. 2002).

Here, the aerosol single-scattering albedo is retrieved from a comparison of the calculated and observed solar irradiance. Figure 4 shows a comparison of measured and calculated direct, diffuse, and total surface irradiances. For the simulations a constant value of the single-scattering albedo of 0.85 was assumed, for which both the direct and diffuse fluxes showed best agreement with the observed values. Each data point in Fig. 4 represents an average over a 10-min time interval. Calculated and measured direct fluxes are in very good agreement, with a slope of 1.03 and a correlation coefficient R^2 of 0.98. The diffuse flux is calculated from the difference between the measured total and direct fluxes and is therefore influenced by the directional response of the pyranometer at high zenith angles. The lower correlation coefficient of the calculated and measured diffuse fluxes might be due to the fact that we assumed constant values of g and ω_0 and did not account for changing aerosol size distributions during the validation period.

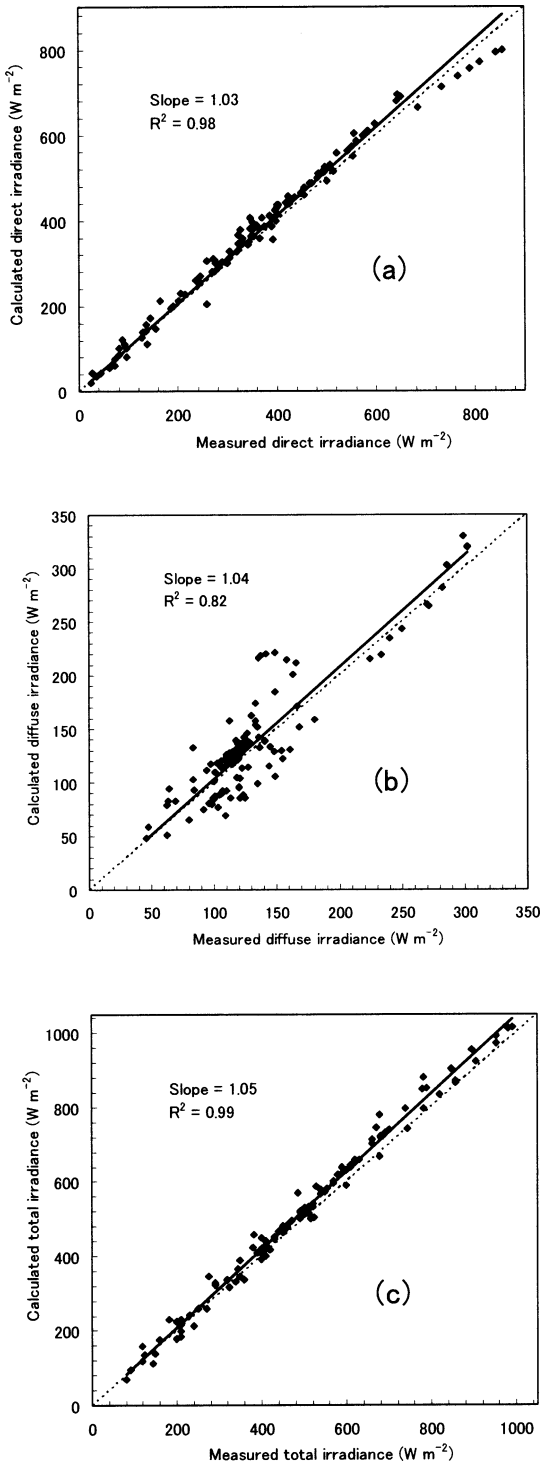

FIG. 4. Comparison of measured and calculated (a) direct, (b) diffuse, and (c) total solar irradiance (W m^{-2}) for 8 days of observation at Kyoto. Data points represent an average value over a 10-min time interval.

5. Discussion

a. Surface aerosol radiative forcing

Surface aerosol radiative forcing was calculated for 21 clear-sky days at Kyoto. An example of the temporal

Unauthenticated | Downloaded 05/06/21 04:29 AM UTC

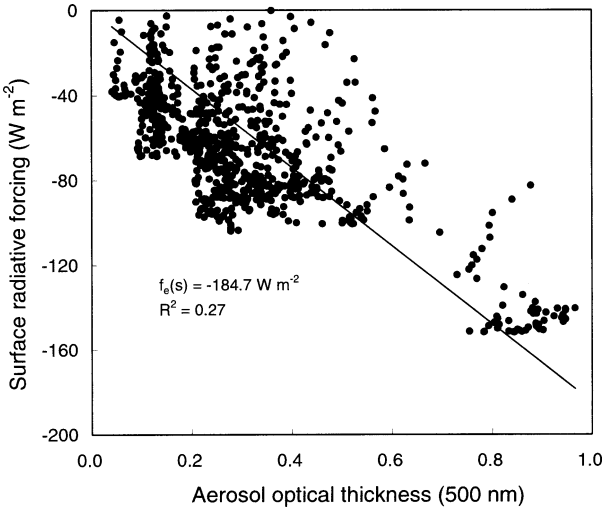

FIG. 5. Scatterplot of the aerosol optical thickness (500 nm) vs instantaneous surface radiative forcing (W m^{-2}). Data points represent an average value over a 10-min time interval.

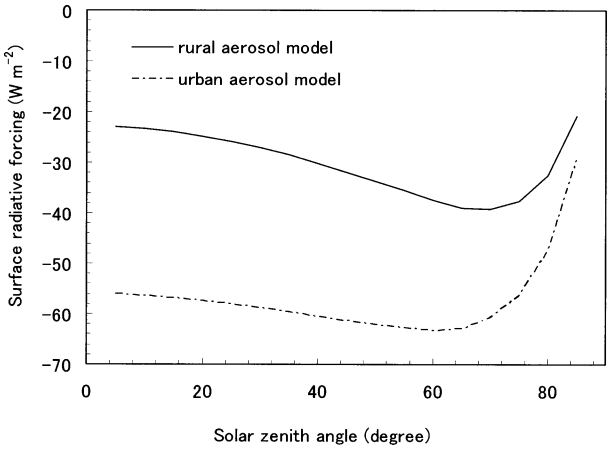

FIG. 6. Relationship between the solar zenith angle and the calculated instantaneous radiative forcing for $\tau_{a,500} = 0.27$, which is the average value at Kyoto.

change of observed and calculated total irradiance is shown in Fig. 3. It can be clearly seen that the atmospheric aerosols act to decrease the downwelling total irradiance. A scatterplot of the aerosol optical thickness $\tau_{a,500}$ versus the instantaneous surface radiative forcing is shown in Fig. 5. The low correlation results from the fact that the surface aerosol radiative forcing is not only sensitive to the aerosol optical properties, but also to the solar zenith angle. In Fig. 6 we investigated the sensitivity of the surface radiative forcing to the solar zenith angle for a constant aerosol optical thickness $\tau_{a,500}$ of 0.27, which is the annual average value at Kyoto. The analysis is carried out for both the default urban and the rural aerosol models, and a strong dependence, especially for high zenith angles, can be seen. It is therefore clear that the correlation between the aerosol optical thickness and the surface forcing is not very high for instantaneous values, as shown in Fig. 5, because of the dominant dependence of ΔF_s on the solar zenith angle. Figure 6 also implies that it is difficult to ''normalize'' the instantaneous surface radiative forcing, because the zenith angle dependence of the surface radiative forcing also depends on the applied aerosol model. The slope in Fig. 5 is called the radiative forcing efficiency f_e, which is the radiative forcing for unit optical thickness. The instantaneous radiative forcing efficiency at the surface $f_e(s)$ at Kyoto is -184.7 W m^{-2}, which lies between the forcing efficiencies of the rural (-121.4 W m^{-2}) and urban (-224.9 W m^{-2}) aerosol models of MODTRAN4. The zenith angle was set at 55° for the calculation, which is an annual average value for Kyoto. From Fig. 5 it can also be seen that the instantaneous aerosol forcing at Kyoto reaches values as high as -150 W m^{-2}.

At one location it is more representative to consider the diurnally averaged radiative forcing $\Delta\overline{F}$ of the aerosol, which is calculated from

$$\Delta\overline{F} = \int \Delta F_s(t)\, dt. \tag{6}$$

The integration is performed over a 24-h time period, which correctly accounts for the daylight fraction at a specific location. To account for very high zenith angles, a polynomial fitted to the measured irradiance time series is extrapolated. The daytime-averaged aerosol optical properties and surface radiative forcings are shown in Table 1; a scatterplot of the daytime-averaged aerosol optical thickness versus surface radiative forcing is shown in Fig. 7. Also shown in Fig. 7 are the diurnal

TABLE 1. Daytime-averaged aerosol optical thickness $\tau_{\alpha,500}$, Ångström exponents α, and diurnally averaged surface radiative forcing ΔF_s.

Date	$\tau_{\alpha,500}$	α	ΔF_s (W m^{-2})
5 Jan 1999	0.20	1.76	−12.8
9 Feb 1999	0.36	1.73	−21.7
16 Feb 1999	0.49	1.60	−33.7
15 May 1999	0.36	1.27	−26.7
29 Aug 1999	0.11	2.72	−17.1
22 Nov 1999	0.43	1.59	−25.5
31 Dec 1999	0.27	1.35	−17.6
19 Jan 2000	0.23	1.51	−15.1
5 Feb 2000	0.35	1.41	−18.3
20 Sep 2000	0.28	2.21	−33.4
23 Apr 2001	0.29	0.72	−44.3
26 Apr 2001	0.34	0.93	−40.0
12 Sep 2001	0.06	1.85	−10.9
20 Sep 2001	0.23	1.48	−32.2
15 Oct 2001	0.26	1.43	−27.5
19 Oct 2001	0.13	1.69	−18.9
30 Oct 2001	0.24	1.39	−21.6
31 Oct 2001	0.24	1.55	−21.8
21 Nov 2001	0.13	1.64	−13.5
12 Dec 2001	0.13	1.62	−10.1
16 Dec 2001	0.13	1.35	−12.3

Unauthenticated | Downloaded 05/06/21 04:29 AM UTC

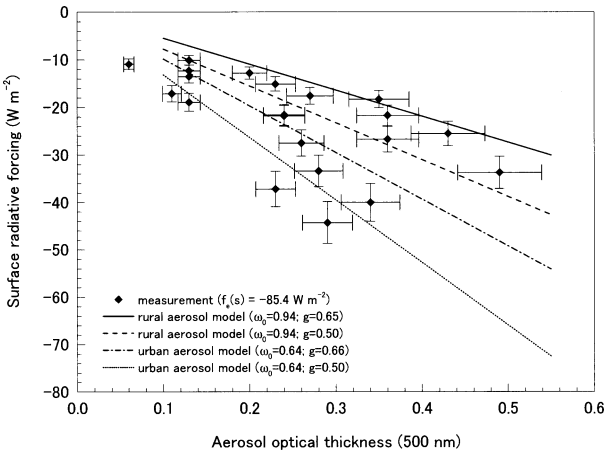

FIG. 7. Scatterplot of the diurnally averaged aerosol optical thickness (500 nm) and surface aerosol radiative forcing. Measured forcings are compared with modeled forcing efficiencies for a rural and an urban aerosol model with given optical properties.

average radiative forcings for the urban and rural aerosol models. The models with asymmetry parameters g of 0.65 and 0.66 are the default models of MODTRAN4, but we also show model results using a lower value of 0.50 for g. It can be seen that the forcing efficiency is highly sensitive to both ω_0 and g. About one-half of the data lie between the theoretical calculations of the default urban ($g = 0.66$) and rural ($g = 0.65$) aerosol models. However, even for an urban aerosol model with a very low asymmetry parameter of $g = 0.50$, there are a few days of measurements with exceptionally high forcing efficiencies lying below this theoretical prediction. We expect that this might be due to a very low single-scattering albedo, which frequently occurs at Kyoto (Höller et al. 2000). No dependency of the surface radiative forcing was found with regard to season or aerosol type for the data in Fig. 7. The complex mixture and large variety of sources of the atmospheric aerosol at this urban location makes a classification of the aerosol with regard to source, season, and so on extremely difficult. Even total aerosol mass concentrations did not show any correlation to wind speed or wind direction at this site. Therefore, to find a correlation between aerosol radiative effects and aerosol sources is even more unlikely.

A linear fit to the measurements gives a daily average broadband aerosol radiative forcing efficiency of −85.4 W m^{-2} (Fig. 7). This value is comparable to that found by Podgorny et al. (2000) in the Indian Ocean during INDOEX (−82 W m^{-2}); those observed during ACE-Asia by Bush and Valero (2001) at Cheju Island, Korea (−82.6 W m^{-2}); and those noted Höller et al. (2001) at a background site on the coast of the Sea of Japan (−80.3 W m^{-2}). It is interesting to note that our data do not lie as clearly on a straight line as the observations of Podgorny et al. (2000). This might be due to the fact that the aerosol at the urban site of Kyoto is much more heterogeneous, with a large variation in its optical and chemical properties. The aerosol measured by Podgorny et al. (2000), described in greater detail with regard to its composition in Satheesh et al. (1999), has a much more stable size distribution and composition, and, therefore, the values of g and ω_0 do not change as much as they do in Kyoto.

For an error analysis of the aerosol optical thickness, we consider errors of the calibration constants of the sun photometer, the measured voltage, and the Rayleigh optical thickness, employing a standard error propagation theory. Because the error of the optical thickness also depends on the solar zenith angle, daytime average error bars are shown in Fig. 7. To estimate the error of the surface aerosol radiative forcing, we considered errors of the columnar water vapor amount from GPS measurements, uncertainties in the atmospheric temperature profiles, and measurement errors of the pyranometer. Nonlinearity in the response of the pyranometer was not considered in the error analysis, because an extrapolated fitting function was used for high zenith angles, for which measurement errors are larger. The error bars in Fig. 7 are calculated for a solar zenith angle of 55°, and the resulting error of the observed surface radiative forcing is 10%.

b. TOA aerosol radiative forcing and atmospheric heating

TOA aerosol radiative forcing can be observed from the measured upwelling flux at the TOA by satellites (Satheesh and Ramanathan 2000). Here we do not directly measure ΔF_{TOA}, but estimate it from radiative transfer calculations using average aerosol properties observed at Kyoto. As mentioned above, aerosol optical properties at Kyoto vary from day to day, which makes it difficult to accurately estimate ΔF_{TOA}. To estimate the average TOA aerosol radiative forcing at Kyoto we employ a single-scattering albedo value of 0.85, which we found to reproduce the diffuse flux at the surface for several days of measurements (see Fig. 4). Moreover, a value of 0.85 of the single-scattering albedo was also found to be an average value over about 30 days of in situ measurements at Kyoto (Höller et al. 2000). For the asymmetry parameter g we employ a value of 0.65 (see section 4b). Using these optical properties and the urban aerosol model size distribution of MODTRAN4, we find a TOA radiative forcing efficiency of −26.9 W m^{-2}, which is about one-third of the observed surface forcing. The use of constant values of the aerosol optical properties does not accurately evaluate the TOA for a specific day but considers average conditions at Kyoto.

Figure 8 shows the relationship between the daytime-averaged aerosol optical thickness and the diurnally averaged TOA radiative forcing, calculated for a surface albedo of 0.15. By way of comparison, we also consider a rural and urban aerosol model with $\omega_0 = 0.94$, $g = 0.50$ and $\omega_0 = 0.64$, $g = 0.70$, respectively. These two

Unauthenticated | Downloaded 05/06/21 04:29 AM UTC

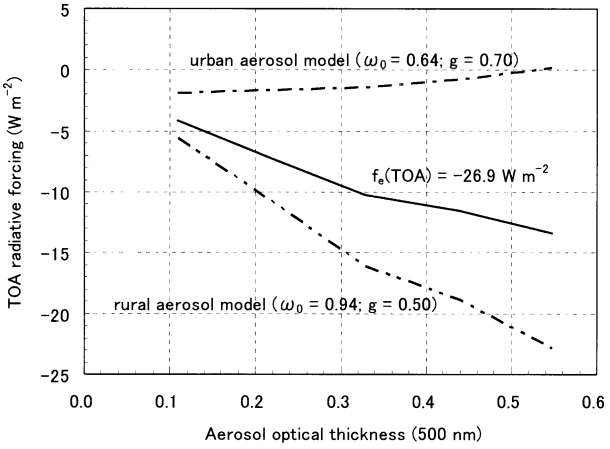

FIG. 8. TOA radiative forcing vs optical thickness (500 nm) calculated for average aerosol optical properties at Kyoto ($\omega_0 = 0.85$; $g = 0.64$). Also shown are the TOA radiative forcings for a rural ($\omega_0 = 0.94$; $g = 0.50$) and an urban aerosol model ($\omega_0 = 0.64$; $g = 0.70$).

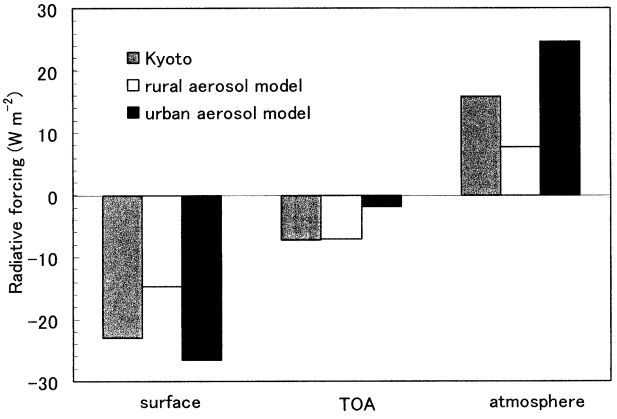

FIG. 9. Surface, TOA, and atmospheric aerosol radiative forcing for $\tau_{a,500} = 0.27$, which is the observed average aerosol optical thickness at Kyoto. Also shown are the radiative forcings for the rural and urban aerosol models.

models represent the two extreme cases of Fig. 7, within which most of the surface measurements lie. It is found that even for the urban model with an asymmetry factor $g = 0.50$, the aerosol produced comprehensive cooling at the TOA for optical thickness values up to 0.54. Considering the observed values of aerosol optical thickness at Kyoto (Fig. 2), it can be seen that τ_a is mostly below this value, resulting in a comprehensive cooling effect at the TOA.

Figure 9 shows a comparison of the radiative forcings at the surface, the TOA, and in the atmosphere. The atmospheric radiative forcing was obtained from the difference between the surface and the TOA forcing. For Kyoto, the surface forcing exceeds the TOA forcing by a factor of about 3, the rural aerosol model by a factor of about 2, and the urban model by a factor of more than 10. This shows the sensitivity of the atmospheric energy budget to the aerosol single-scattering albedo. Whereas for conservatively scattering (i.e., nonabsorbing) particles the TOA forcing and the surface forcing are the same, absorbing aerosols produce a cooling at the surface and a heating of the atmosphere. In comparison with the rural and urban aerosol models, the aerosol at Kyoto lies somewhere between these limiting cases with regard to the surface and atmospheric radiative forcings.

6. Conclusions

Continuous measurements of surface solar irradiance and columnar aerosol optical properties were made during the period from September 1998 to December 2001. We observed high variability in aerosol optical thickness ranging from 0.06 to 0.83. Ångström exponents, which had values from 0.52 to 2.79, indicate a high variability of the aerosol size distribution at this site. Observations of surface solar irradiances were carried out to validate radiative transfer calculations, which were then used to estimate the TOA radiative forcing of the aerosol. We found the best agreement between calculated and measured surface diffuse fluxes to be for a single-scattering albedo value of 0.85. The surface aerosol radiative forcing was obtained from observed broadband total surface irradiances and calculated no-aerosol fluxes. A surface radiative forcing efficiency of -85.4 W m^{-2} was found as an average value for 21 near-clear-sky days. This value is similar to an earlier measured radiative forcing efficiency of -80.3 W m^{-2} at a background site on the coast of the Sea of Japan. Measurements in the Indian Ocean and Korea gave similar values, which indicate that a value of -85 ± 5 W m^{-2} might represent a general broadband aerosol forcing efficiency that does not depend strongly on the chemical composition of the aerosol.

We have discussed the impact of the aerosol on redistribution of the solar fluxes among the surface, TOA, and atmosphere. For that purpose, the aerosol single-scattering albedo was retrieved from a comparison of measured and simulated solar irradiance at the surface. We found that the surface aerosol radiative forcing exceeds the TOA forcing by a factor of about 3, which is due to the low single-scattering albedo, and that absorbing aerosols produce a large amount of atmospheric heating. An error analysis showed that the surface radiative forcings obtained here have an error of about 10%. To further reduce this error, it will be necessary to have continuous information of changes in the aerosol size distribution and measured vertical profiles of aerosol optical properties. Further studies will be necessary to reduce these uncertainties and also to estimate the overall aerosol radiative impact, which should include the indirect effect through changing cloud properties.

Acknowledgments. This work was partly supported by funds from the ''Research for the Future'' (RFTF) program of the Japan Society for the Promotion of Sci-

Unauthenticated | Downloaded 05/06/21 04:29 AM UTC

ence (JSPS-RFTF 97P01002), and from the Grant-in-Aid for Scientific Research (B) 09044161 from the Ministry of Education, Science, Sports and Culture, Japan. Helpful comments from J. P. Matthews of Kyoto University are gratefully acknowledged. We also thank Brett C. Bush and an anonymous reviewer for their insightful comments and suggestions.

REFERENCES

Berk, A., and Coauthors, 1999: MODTRAN4 radiative transfer modeling for atmospheric correction. *Proc. SPIE, Opt. Spectroscop. Tech. Instrum. Atmos. Space Res. III,* **3756,** 348–353.

Bush, B. C., and F. P. J. Valero, 2001: Total column radiative forcing by aerosols during the ACE-Asia campaign. *Eos, Trans. Amer. Geophys. Union,* **82** (Abstract A41B-0071), F93.

——, and ——, 2002: Spectral aerosol radiative forcing at the surface during the Indian Ocean Experiment (INDOEX). *J. Geophys. Res.,* **107,** 8003, doi:10.1029/2000JD000020.

——, ——, A. S. Simpson, and L. Bignone, 2000: Characterization of thermal effects in pyranometers: A data correction algorithm for improved measurements of surface insolation. *J. Atmos. Oceanic Technol.,* **17,** 165–175.

Charlson, R. J., S. E. Schwartz, J. M. Hales, R. D. Cess, J. A. Coakley, J. E. Hansen, and D. J. Hoffmann, 1992: Climate forcing by anthropogenic aerosols. *Science,* **255,** 423–430.

Chylek, P., and J. A. Coakley, 1974: Aerosols and climate. *Science,* **183,** 75–77.

Conant, W. C., V. Ramanathan, F. P. J. Valero, and J. Meywerk, 1997: An examination of the clear-sky solar absorption over the central equatorial Pacific: Observation versus models. *J. Climate,* **10,** 1874–1884.

Flowers, E. C., R. A. McCormick, and K. R. Kurfis, 1969: Atmospheric turbidity over the United States, 1961–1966. *J. Appl. Meteor.,* **8,** 955–962.

Hansen, J. E., M. Sato, and R. Ruedy, 1997: Radiative forcing and climate response. *J. Geophys. Res.,* **102,** 6831–6864.

Hayasaka, T., N. Kikuchi, and M. Tanaka, 1995: Absorption of solar radiation by stratocumulus clouds: Aircraft measurements and theoretical calculations. *J. Appl. Meteor.,* **34,** 1047–1055.

Haywood, J. M., and K. P. Shine, 1995: The effect of anthropogenic sulfate and soot aerosol on the clear sky planetary radiation budget. *Geophys. Res. Lett.,* **22,** 603–606.

Hignett, P., J. P. Taylor, P. N. Francis, and M. D. Glew, 1999: Comparison of observed and modeled direct radiative forcing during TARFOX. *J. Geophys. Res.,* **104,** 2279–2287.

Hirose, K., Y. Dokiya, and Y. Sugimura, 1983: Effect of the continental dust over the north Pacific Ocean: Time variation of chemical components in maritime aerosol particles in spring season. *J. Meteor. Soc. Japan,* **61,** 670–677.

Holben, B. N., and Coauthors, 2001: An emerging ground-based aerosol climatology: Aerosol optical depth from the AERONET. *J. Geophys. Res.,* **106,** 12 067–12 097.

Höller, R., 2000: Studies of the optical properties and climatic relevance of the atmospheric aerosol in Japan. Ph.D. dissertation, Kyoto University, Kyoto, Japan, 143 pp. [Available from Kyoto University, Yoshida-Honmachi, Sakyo, Kyoto 606-8501, Japan.]

——, M. Kasahara, and H. Horvath, 2000: Aerosol single-scattering albedo determined by horizontal extinction closure. *J. Aerosol Res. Japan,* **15,** 246–255.

——, T. Yabe, S. Tohno, and M. Kasahara, 2001: Aerosol radiative effects observed on the coast of the Japanese Sea (Tango peninsula) during ACE-Asia. *Eos, Trans. Amer. Geophys. Union,* **82** (Abstract A21A-0026), F48.

——, S. Tohno, M. Kasahara, and R. Hitzenberger, 2002: Long-term characterization of carbonaceous aerosol at Uji, Japan. *Atmos. Environ.,* **36,** 1267–1275.

Horvath, H., 1993: Atmospheric light absorption—A review. *Atmos. Environ.,* **27A,** 293–317.

Houghton, J. T., Y. Ding, D. J. Griggs, M. Noguer, P. J. van der Linden, X. Dai, K. Maskell, and C. A. Johnson, Eds., 2001: *Climate Change 2001: The Scientific Basis: Contribution of Working Group I to the Third Assessment Report of the Intergovernmental Panel on Climate Change,* Cambridge University Press, 881 pp.

Iqbal, M., 1983: *An Introduction to Solar Radiation.* Academic Press, 390 pp.

Iwasaka, Y., H. Minoura, and K. Nagaya, 1983: The transport and spatial scale of Asian dust-storm clouds; A case study of the dust-storm event of April 1979. *Tellus,* **35B,** 189–196.

Japan Meteorological Agency, 2002: Annual report of ozone layer monitoring: 2001 (in Japanese). 54 pp. [Available from Japan Meteorological Agency, Otemachi, Chiyoda, Tokyo 100-8122, Japan.]

Kasahara, M., T. Chatani, S. Tohno, and R. Höller, 1999: Physical and chemical characteristics of atmospheric aerosols in Kyoto. *J. Aerosol Sci.,* **30** (Suppl. 1), 257–258.

Kondratyev, K. Y., 1969: *Radiation in the Atmosphere.* Academic Press, 567 pp.

Liao, H., and J. H. Seinfeld, 1998: Radiative forcing by mineral dust aerosols: Sensitivity to key variables. *J. Geophys. Res.,* **103,** 31 637–31 645.

Marshall, S. F., D. S. Covert, and R. J. Charlson, 1995: Relationship between asymmetry parameter and hemispheric backscatter ratio: Implications for climate forcing by aerosol. *Appl. Opt.,* **34,** 6306–6311.

Nakajima, T., T. Hayasaka, A. Higurashi, G. Hashida, N. Moharram-Nejad, Y. Najafi, and H. Valavi, 1996: Aerosol optical properties in the Iranian region obtained by ground-based solar radiation measurements in the summer of 1991. *J. Appl. Meteor.,* **35,** 1265–1278.

Ohta, S., and T. Okita, 1984: Measurements of particulate carbon in urban and marine air in Japanese areas. *Atmos. Environ.,* **18,** 2439–2445.

Pilinis, C., S. N. Pandis, and J. H. Seinfeld, 1995: Sensitivity of direct climate forcing by atmospheric aerosols to aerosol size and composition. *J. Geophys. Res.,* **100,** 739–754.

Podgorny, I. A., W. Conant, V. Ramanathan, and S. K. Satheesh, 2000: Aerosol modulation of atmospheric and surface solar heating over the tropical Indian Ocean. *Tellus,* **52B,** 947–958.

Ramanathan, V., and Coauthors, 2001: The Indian Ocean Experiment: An integrated analysis of the climate forcing and effects of the great Indo-Asian haze. *J. Geophys. Res.,* **106,** 28 371–28 398.

Russell, P. B., and Coauthors, 1999: Aerosol-induced radiative flux changes off the United States mid-Atlantic coast: Calculations of values calculated from sunphotometer and in situ data with those measured by airborne pyranometer. *J. Geophys. Res.,* **104,** 2284–2307.

Satheesh, S. K., and V. Ramanathan, 2000: Large differences in tropical aerosol forcing at the top of the atmosphere and earth's surface. *Nature,* **405,** 60–63.

——, ——, X. Li-Jones, J. M. Lobert, I. A. Podgorny, J. M. Prospero, B. N. Holben, and N. G. Loeb, 1999: A model for the natural and anthropogenic aerosols over the tropical Indian Ocean derived from Indian Ocean Experiment data. *J. Geophys. Res.,* **104,** 27 421–27 440.

Schwartz, S. E., 1996: The whitehouse effect—Shortwave radiative forcing of climate by anthropogenic aerosols: An overview. *J. Aerosol Sci.,* **27,** 359–382.

Takemura, T., T. Nakajima, O. Dubovik, B. Holben, and S. Kinne, 2002: Single-scattering albedo and radiative forcing of various aerosol species with a global three-dimensional model. *J. Climate,* **15,** 333–352.

Tregoning, P., R. Boers, D. O'Brien, and M. Hendy, 1998: Accuracy of absolute precipitable water estimates from GPS observations. *J. Geophys. Res.,* **103,** 28 701–28 710.

Young, A. T., 1981: On the Rayleigh-scattering optical depth of the atmosphere. *J. Appl. Meteor.,* **20,** 328–329.

Unauthenticated | Downloaded 05/06/21 04:29 AM UTC